Mesoscopic Void Structures in Cobalt Nanocrystal Films Formed from Drying Concentrated Colloidal Solutions

C. Salzemann,[1] J. Richardi,[1] I. Lisiecki,[1] J.-J. Weis,[2] and M. P. Pileni[1]

[1]*Laboratoire des Matériaux Mésoscopiques et Nanométriques, U.M.R. C.N.R.S. 7070, Université Pierre et Marie Curie (Paris VI), BP. 52, 75230 Paris Cedex 05, France*

[2]*Laboratoire de Physique Théorique, UMR8627, Université de Paris XI, Bâtiment 210, 91405 Orsay Cedex, France*

(Received 12 August 2008; published 7 April 2009)

Here we report the formation of void (hole) structures when concentrated colloidal solutions of magnetic nanocrystals are subjected to a magnetic field during slow evaporation. This presents a new type of solid mesostructure obtained by self-assembly of nanocrystals. The voids are characterized by a cylindrical shape with either circular or elliptical base. We show that the morphology of these patterns is essentially controlled by the fraction of the volume occupied by the magnetic phase to the total volume of the film. Monte Carlo simulations carried out using a Stockmayer fluid model agree remarkably well with the experiments for the formation of void structures in the range of considered volume fractions.

DOI: 10.1103/PhysRevLett.102.144502 PACS numbers: 47.54.−r, 47.65.Cb, 77.84.Nh, 83.80.Hj

Formation of domain patterns as arrays of columns or labyrinths with submicron dimensions are observed in a variety of experimental systems like ferrofluids, films of magnetic garnets, diblock copolymers, phospholipid monolayers, superconductors, semiconductors, and Rayleigh Bernard instabilities [1–7]. Recently, mesostructures of hexagonally ordered columns and labyrinths were observed when colloidal solutions of magnetic nanocrystals are subjected to a magnetic field during the evaporation [8–12]. The morphology of these patterns was described by the order parameter Φ defined as the ratio of the volume occupied by the magnetic phase to the total volume of the film after the total evaporation of the solvent [13]. Here, we show, for the first time, to the best of our knowledge, formation, at large Φ values, of void (hole) structures having a cylindrical shape with, depending on Φ, either a circular or a more elliptical base. The experimental fabrication of well defined void structures has become possible due to the successful preparation of highly concentrated stable cobalt nanocrystal solutions. This enables the fabrication of a new type of solid mesostructure by self-assembly of nanoparticles, which is interesting for the community working on self-assembly and nanomaterials.

The synthesis of cobalt nanocrystals coated with dodecanoic acid is described in Ref. [14,15]. The nanocrystals are coated with dodecanoic acid and extracted from the surfactant before being dispersed in hexane. Cobalt nanocrystals have a mean diameter of 7.5 ± 0.1 nm and a 9.8% size dispersion. The cobalt nanocrystals are poorly crystallized with a fcc structure. The saturation magnetization of the nanocrystals isolated in solution (120 emu g^{-1}) is close to the bulk value (166 emu g^{-1}) [16]. Three-dimensional mesostructures with different morphologies are produced by immerging a substrate (either Highly Oriented Pyrolitic Graphite, HOPG, or a silicon wafer, Si) in a colloidal solution of cobalt nanocrystals. Both substrates are wetted by hexane in the same way. To exclude any effect of different types of nanocrystals and of temperature, experiments are carried out with the same batch of nanoparticles and at ambient temperature. The evaporation is slowed down by the use a parafilm which seals the beaker. Former experiments have shown that this decrease of evaporation speed is essential to obtain quasiequilibrium structures [8]. The same 1.4-cm diameter beaker is used for all experiments. The total amount, n, of cobalt nanocrystals in the colloidal solution is controlled by changing the solution concentration (from 5×10^{-4} to 10^{-2} M) and/or the immersion volume (200 μl or 400 μl). More than 50 evaporation experiments on different conditions were carried out. Void structures were found only in a very narrow range of concentrations (5×10^{-3} and 10^{-2} M), while under other conditions, close films or columns were observed. We have restricted our presentation to this narrow range of conditions. During solvent evaporation (about 12 h), a magnetic field is applied perpendicularly to the substrate using a permanent magnet of 0.4 T. To exclude angular distribution of the magnetic field, the magnet used here is large with respect to the substrate. In order to prevent oxidation, the synthesis and fabrication of the samples are done in a glove box. After total evaporation of the solvent, the samples are investigated by Scanning Electron Microscopy (SEM) using a JMS-5510LV instrument. During the evaporation, the volume fraction of nanoparticles increases gradually, and we have shown in a recent publication [10] that close to the end of the evaporation, the system exhibits a colloidal gas-liquid transition. This leads to the coexistence of a concentrated and diluted phase of magnetic nanoparticles. The volume fraction corresponds to the overall fraction of the volume occupied by the concentrated phase to the total volume occupied by both phases. Considering that the void structures have the same thickness as the nanoparticle film, Φ is given by $(S - s)/S$ where S is the surface area of the substrate selected on the SEM image and s the total area of the void regions. The

experiments show that the structures are homogeneous over a larger area. We have chosen the surface area so that it contains a sufficiently large number (>100) of voids and the variation of the void radius is less than 10%. Please note that the experiments described below have been carried out several times and the data are all consistent.

Figures 1(a) and 1(b) show, for different magnifications, the SEM images of the mesostructures obtained on a Si substrate immersed in 200 μl of a 5×10^{-3} M colloidal solution. In this case, circular cylindrical void mesostructures forming a distorted hexagonal network are observed. The average diameter of their circular bases is determined from the SEM images for 150 void structures and found to be (0.33 ± 0.01) μm. For this mesostructure, a volume fraction of 0.91 ± 0.01 is measured. In order to assess the influence of the amount of Co nanocrystals on pattern formation, the same experiment is performed with 400 μl of 5×10^{-3} M solution instead of 200 μl yielding a higher amount of nanocrystals. Figures 1(c) and 1(d) show that the void mesostructures adopt a cylindrical structure with an elliptic-like basis having an aspect ratio around 3.4 and $\Phi = 0.73 \pm 0.02$. The void structures appear to locally orient, on average, in the same direction. Keeping the same amount of cobalt nanocrystals and using a higher concentration of colloidal solution (10^{-2} M), i.e., a smaller immersion volume (200 μl), Figs. 1(e) and 1(f) show that cylindrical voids with a circular base are again observed as in experiment 1 with the conditions: 200 μl, 5×10^{-3} M. However, contrary to the first experiment, no hexagonal network is observed, and the cylindrical structures are not well defined so that an average diameter and volume fraction could not be determined. By replacing Si substrate by HOPG and keeping the same experimental conditions as above (200 μl, 10^{-2} M), two different morphologies are simultaneously observed: cylindrical void mesostructures with circular base characterized by an average diameter of (0.18 ± 0.01) μm and $\Phi = 0.91 \pm 0.01$ and inverted labyrinthine structures with $\Phi = 0.70 \pm 0.04$ [Figs. 1(g) and 1(h)]. Hence, keeping the same experimental conditions and changing the substrate (Si, HOPG), cylindrical voids are observed in both cases whereas the presence of inverted labyrinths is also found on HOPG explained by irregularities of this substrate at a large scale. These results seem somewhat puzzling but can be rationalized by observing that Φ is the relevant parameter for mesostructure morphologies rather than the total amount, n, of cobalt nanocrystals. In fact, during evaporation, nanocrystals can deposit along the beaker walls that depend on the volume of solution. The volume fraction Φ evaluated in the different experiments shows that cylindrical void (circular base) mesostructures correspond to $\Phi = 0.91 \pm 0.01$, for any experimental conditions, to form these mesostructures. When the void morphology evolves from cylindrical void to elliptic cylindrical void mesostructures, the volume fraction decreases from 0.91 to 0.73 ± 0.02. At a still lower volume fraction ($\Phi \approx 0.7$), the elliptic cylindrical mesostructures become more elongated leading to the inversed labyrinthine structures observed on HOPG.

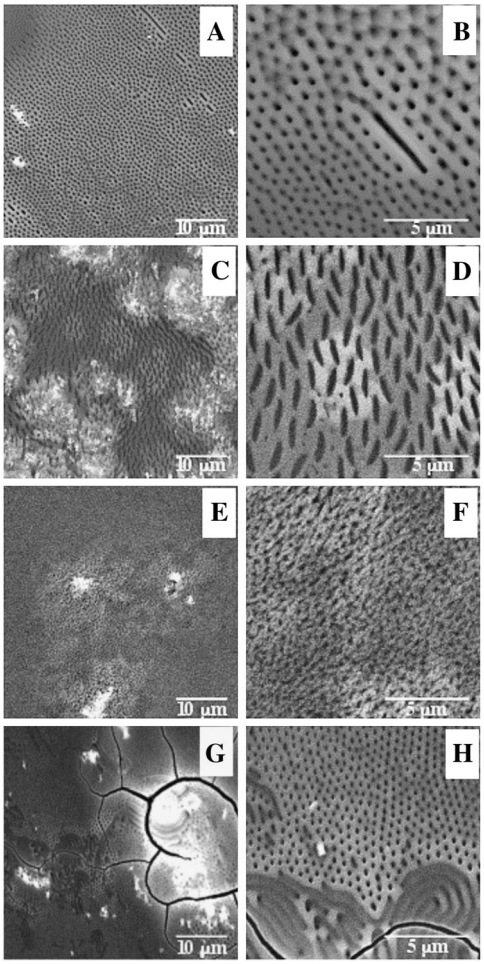

FIG. 1. SEM images of void structures obtained on Si substrate by evaporation of 200 μl of a 5×10^{-3} M concentrated solution (a) and (b), 400 μl of a 5×10^{-3} M concentrated solution (c) and (d), and 200 μl of a 10^{-2} M concentrated solution (e) and (f). SEM images of void structures obtained on HOPG substrate by evaporation of 200 μl of a 10^{-2} M concentrated solution (g) and (h).

The physical origin of the structure lies in the competition between short-range attractive forces and long-range dipolar repulsion between the nanocrystals. A free energy approach taking into account the attractive surface and the repulsive dipolar energies of the structures shows that the void structures are the most stable pattern at large volume fractions [17]. To quantitatively predict the range of the labyrinthine and void phases as a function of volume fraction and field, simulations have to be carried out taking the entropy directly into account. Monte Carlo simulations [18] have been performed in the density range $\rho = 0.4$–0.6 for magnetic fields $H = 3$–30 in reduced units.

The simulations were performed in a similar way as described in our previous work [19]. The interaction between two nanocrystals i and j is described by a Stockmayer pair potential, which consists of a dipole-dipole interaction

$v_{dd}(\boldsymbol{r}_{ij}, \boldsymbol{\mu}_i, \boldsymbol{\mu}_j)$ and a Lennard-Jones (LJ) potential $v_{\mathrm{LJ}}(r_{ij})$ with parameters ε and σ:

$$v_{\mathrm{LJ}}(r_{ij}) = 4\varepsilon\left[\left(\frac{\sigma}{r_{ij}}\right)^{12} - \left(\frac{\sigma}{r_{ij}}\right)^{6}\right] \quad (1)$$

$$v_{dd}(\boldsymbol{r}_{ij}, \boldsymbol{\mu}_i, \boldsymbol{\mu}_j) = \frac{1}{4\pi\mu_0 r_{ij}^3}\left[\boldsymbol{\mu}_i \cdot \boldsymbol{\mu}_j - \frac{3(\boldsymbol{\mu}_i \cdot \boldsymbol{r}_{ij})(\boldsymbol{\mu}_j \cdot \boldsymbol{r}_{ij})}{r_{ij}^2}\right] \quad (2)$$

where $\boldsymbol{\mu}_i = \mu \boldsymbol{s}_j$ and $\boldsymbol{\mu}_j$ are the dipole moments of particles i and j, $\boldsymbol{s}_i$ the unit vector in the direction of the dipole moment, $\boldsymbol{r}_{ij} = \boldsymbol{r}_j$-$\boldsymbol{r}_i$ the vector joining the centers of mass of the particles, $r_{ij} = |\boldsymbol{r}_{ij}|$ and $\mu_0 = 4\pi 10^{-7}\ \mathrm{J\,A^{-2}\,m^{-1}}$ the permeability of vacuum. The magnetic dipole μ is calculated from the bulk magnetization M_d ($M_d = 14 \times 10^5\ \mathrm{A\,m^{-1}}$ for cobalt) according to $\mu = \mu_o M_d (\pi/6) {d_m}^3$. Using a value of 8 nm for the average magnetic diameter d_m of the cobalt nanocrystal yields a reduced dipole moment $\mu^* = \mu/\sqrt{(\varepsilon\sigma^3 4\pi\mu_0)} = 2$. In order to model the thin film which appears during the evaporation of the nanocrystal solution, the Stockmayer fluid is confined between two parallel walls separated by a distance $L/\sigma = 10$. Structure morphologies do not depend markedly on L except for very small values. The particle-wall interaction is purely repulsive decaying $1/z^{12}$ where z is the distance of a particle from the wall. Since pattern formation is experimentally associated with a gas-liquid transition, densities and temperatures were chosen within the gas-liquid coexistence region of the Stockmayer fluid. The reduced temperature was fixed at $T^* = kT/\varepsilon = 1.25$. Values for the strength of the magnetic field, applied perpendicularly to the walls, were $H^* = H\sqrt{\varepsilon\sigma^3} = 5$, 10, 20, 30 corresponding to 0.09, 0.18, 0.36, and 0.545 T, respectively. The MC simulations were performed in the canonical ensemble [18] using $N = 2592$ or $N = 3000$ particles with periodic boundary conditions in the x and y directions parallel to the walls. The long-range dipolar interactions were taken into account by a modified, slab-adapted Ewald sum [20–22]. Typical simulation runs involved 1.8×10^6 cycles after equilibration of the system, a cycle corresponding to translation and rotation of the N particles. For notational convenience, stars in the reduced quantities will be omitted in the remainder of the Letter.

The MC results obtained for $\rho = 0.4$–0.6 can be combined with our previous MC results [19] covering the density range $\rho = 0.1$–0.4. Thus, a full sequence of microstructures is found: they range from cylindrical columns arranged in a near hexagonal array to vertical sheetlike labyrinths and finally to hole (void) structures. Monte Carlo simulations carried out without the attractive van der Waals term did not yield any structures such as columns, labyrinths, or voids. Fixing the value of H at 30 (corresponding to 0.545 Tesla), simulations are performed at various densities. Figure 2 shows cylindrical columns for $\rho = 0.1$ [Fig. 2(a)], vertical sheetlike labyrinths are observed at $\rho = 0.3$ [Fig. 2(b)] and void structures for $0.4 < \rho < 0.55$ (Figs. 2(d)–2(i)). Extended simulations at various field and density values allows sketching the different phases obtained from the MC simulations of the confined Stockmayer fluid as a function of density and field strength in Fig. 3. Figure 2 gives a more detailed description of the region of void microstructures: For $H \leq 5$ (i.e., $H \leq 0.09$ Tesla), the system behaves as a nearly homogeneous drop typical of gas-liquid coexistence [Fig. 2(c)]. Elongated holes start to appear at $\rho \approx 0.4$ for $H \geq 5$ [Figs. 2(d) and 2(e)] and first coexist with the sheetlike structures typical of the lower densities. With increasing density these elongated (elliptical-like) holes become smaller and for densities $\rho > 0.45$ (circular) cylindrical void structures arranged in a somewhat distorted hexagonal array are obtained [Fig. 2(f)–2(i)]. The diameter of the void cylinders decreases as a function of the density from $\rho = 0.45$ [Fig. 2(f)] to $\rho = 0.55$ [Fig. 2(i)]. This type of organization corresponds to the inverted hexagonal structure predicted by free energy approaches [17]. Quite remarkably, these hole structures are by no means static but migrate through the system on a rather rapid "time" scale. At $\rho = 0.6$, where the confined Stockmayer system approaches the liquid region in zero field (cf. phase diagram in Fig. 1 of Ref. [19]), the system is too dense for voids to form and the particles fill the simulation box in a nearly homogeneous way. To make a more quantitative comparison of the conditions for onset of the different morphologies with experiment, we calculated the volume fraction Φ,

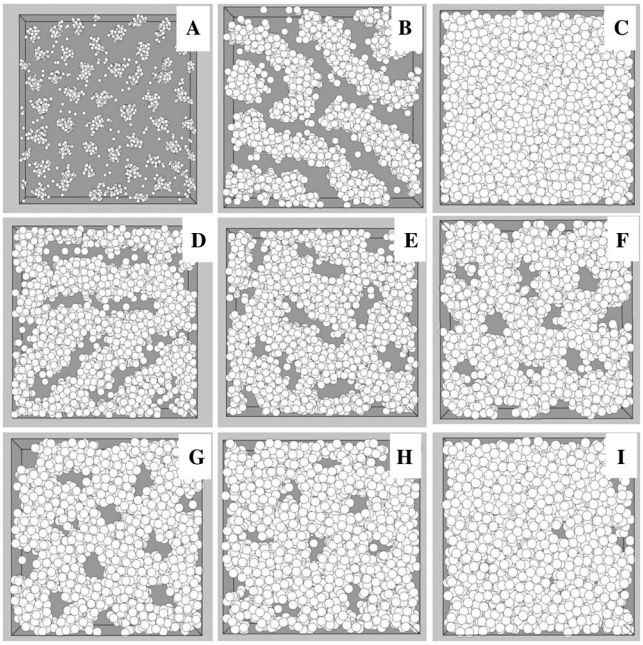

FIG. 2. Snapshots of particle configurations of the confined Stockmayer fluid at $T = 1.25$, $\mu = 2.0$, and $L = 10$: (a) $\rho = 0.1$, $H = 30$; (b) $\rho = 0.3$, $H = 30$; (c) $\rho = 0.4$, $H = 5$; (d) $\rho = 0.4$, $H = 30$; (e) $\rho = 0.42$, $H = 30$; (f) $\rho = 0.45$, $H = 30$; (g) $\rho = 0.48$, $H = 30$; (h) $\rho = 0.5$, $H = 30$; (i) $\rho = 0.55$, $H = 20$; $N = 3000$ except for figures (a), (f)–(i) $N = 2592$.

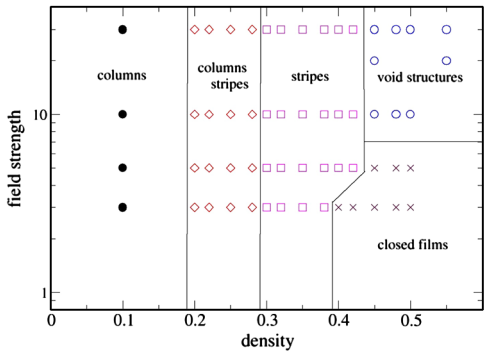

FIG. 3 (color online). Sketch of the phase behavior of the confined Stockmayer system predicted by Monte Carlo simulation as a function of density and field strength. The symbols represent the different simulated state points considered: filled circles: columnar phase; diamonds: coexistence of columns and sheets; squares: sheets (labyrinths); open circles: void structures; crosses: homogeneous film. The state points for $\rho < 0.4$ are from Ref. [19].

defined as the ratio of the surface occupied by the aggregates and the simulation box. The analysis is restricted to fields $20 < H < 30$ (corresponding to $0.36 < H < 0.545$ Tesla) as in the experiments. Within the statistical error, results for Φ turn out not to depend appreciably on H for $H = 10$–30. At $\rho = 0.45$, one finds $\Phi = 0.83 \pm 0.03$. Simulations thus predict the formation of void cylinders at a volume fraction larger than 0.83 in fair agreement with experiment where these structures are observed at $\Phi = 0.91 \pm 0.01$. Elliptical holes are obtained in the simulations at densities between 0.4 and 0.45, i.e., for volume fractions between $\Phi = 0.70 \pm 0.03$ and 0.83 ± 0.03, which also well fits the experimental value of 0.73 ± 0.03. Molecular dynamics simulations have been performed recently for a similar system and nearly identical parameters but for the higher density $\rho = 0.6$, which corresponds to a liquid density (outside to the liquid-gas coexistence region of the Stockmayer potential in zero field). At this density, layering of the particles is observed for suitable separations of the confining surfaces ($h \leq 5$) [23]. To conclude, contrary to former experiments where only columns and labyrinths were obtained, void structures in cobalt nanocrystal films are here observed for the first time due to the use of stable concentrated colloidal solutions of cobalt nanocrystals. These structures are characterized by a higher volume fraction than 0.7 of cobalt deposited on the substrate in excellent agreement with the values predicted by our MC simulations. Both experimental and theoretical results show that the volume fraction (and not the initial conditions of the experiment) is the key factor to explain the appearance of void structures. In addition, a change in Φ changes the morphology of the voids. Finally, one can note that in recent computer simulations, inverse phases have been shown to arise even in very simple systems (spherically symmetrical potentials) from competition in the length scales of attractive and repulsive interactions between the particles [24–26]. This shows that the kind of void structures observed here experimentally for the first time can be expected in a large variety of other systems.

We thank Drs. C. Petit and D. Ingert for fruitful discussions on their observations of mesostructures in cobalt nanocrystal films.

[1] M. Seul and D. Andelman, Science **267**, 476 (1995).
[2] J. A. Cape and G. W. Lehman, J. Appl. Phys. **42**, 5732 (1971).
[3] R. M. Weis and H. M. McConnell, Nature (London) **310**, 47 (1984).
[4] E. N. Thomas, D. M. Anderson, C. S. Henke, and D. Hoffman, Nature (London) **334**, 598 (1988).
[5] H. Hasegawa and T. Hashimoto, Polymer **33**, 475 (1992).
[6] R. E. Rosensweig, M. Zahn, and R. Shumovich, J. Magn. Magn. Mater. **39**, 127 (1983).
[7] J. C. Bacri, R. Perzynski, and D. Salin, Endeavour, New Series **12**, 76 (1988).
[8] J. Legrand, A. T. Ngo, C. Petit, and M. P. Pileni, Adv. Mater. **13**, 58 (2001).
[9] G. Leo, Y. Chushkin, S. Luby, E. Majkova, I. Kostic, M. Ulmeanu, A. Luches, M. Giersig, and M. Hilgendorff, Mater. Sci. Eng., C **23**, 949 (2003).
[10] V. Germain, J. Richardi, D. Ingert, and M. P. Pileni, J. Phys. Chem. B **109**, 5541 (2005).
[11] V. Germain and M. P. Pileni, Adv. Mater. **17**, 1424 (2005).
[12] A. T. Ngo, J. Richardi, and M. P. Pileni, Langmuir **21**, 10234 (2005).
[13] J. Richardi, D. Ingert, and M. P. Pileni, Phys. Rev. E **66**, 046306 (2002).
[14] I. Lisiecki and M. P. Pileni, Langmuir **19**, 9486 (2003).
[15] C. Petit, P. Lixon, and M. P. Pileni, Langmuir **7**, 2620 (1991).
[16] V. Russier, C. Petit, and M. P. Pileni, J. Appl. Phys. **93**, 10001 (2003).
[17] D. Lacoste and T. C. Lubensky, Phys. Rev. E **64**, 041506 (2001).
[18] M. P. Allen and D. J. Tildesley, *Computer Simulation of Liquids* (Clarendon, Oxford, 1989).
[19] J. Richardi, M. P. Pileni, and J. J. Weis, Phys. Rev. E **77**, 061510 (2008).
[20] I. C. Yeh and M. L. Berkowitz, J. Chem. Phys. **111**, 3155 (1999).
[21] J. C. Shelley and G. N. Patey, Mol. Phys. **88**, 385 (1996).
[22] S. H. L. Klapp and M. Schoen, J. Chem. Phys. **117**, 8050 (2002).
[23] J. Jordanovic and S. H. L. Klapp, Phys. Rev. Lett. **101**, 038302 (2008).
[24] A. J. Archer and N. B. Wilding, Phys. Rev. E **76**, 031501 (2007).
[25] A. J. Archer, Phys. Rev. E **78**, 031402 (2008), and references therein.
[26] M. A. Glaser, G. M. Grason, R. D. Kamien, A. Kosmrlj, C. D. Santangelo, and P. Ziherl, Europhys. Lett. **78**, 46004 (2007).